The Astrophysical Journal, 901:165 (9pp), 2020 October 1 https://doi.org/10.3847/1538-4357/abb1a8

Simultaneous X-Ray and Radio Observations of the Repeating Fast Radio Burst FRB ∼ 180916.J0158+65

P. Scholz[1], A. Cook[1], M. Cruces[2], J. W. T. Hessels[3,4], V. M. Kaspi[5,6], W. A. Majid[7,8], A. Naidu[5,6], A. B. Pearlman[8,19,20], L. G. Spitler[2], K. M. Bandura[9,10], M. Bhardwaj[5,6], T. Cassanelli[1], P. Chawla[5,6], B. M. Gaensler[1], D. C. Good[11], A. Josephy[5,6], R. Karuppusamy[2], A. Keimpema[12], A. Yu. Kirichenko[13,14], F. Kirsten[15], J. Kocz[8], C. Leung[16,17], B. Marcote[12], K. Masui[16,17], J. Mena-Parra[16], M. Merryfield[5,6], D. Michilli[5,6], C. J. Naudet[7], K. Nimmo[3,4], Z. Pleunis[5,6], T. A. Prince[7,8], M. Rafiei-Ravandi[18], M. Rahman[1], K. Shin[16,17], K. M. Smith[18], I. H. Stairs[11], S. P. Tendulkar[5,6], and K. Vanderlinde[1]

[1] Dunlap Institute for Astronomy & Astrophysics, University of Toronto, 50 St. George Street, Toronto, ON M5S 3H4, Canada; paul.scholz@dunlap.utoronto.ca
[2] Max Planck Institut für Radioastronomie, Auf dem Hügel 69, D-53121, Bonn, Germany
[3] Anton Pannekoek Institute for Astronomy, University of Amsterdam, Science Park 904, 1098 XH, Amsterdam, The Netherlands
[4] ASTRON, Netherlands Institute for Radio Astronomy, Oude Hoogeveensedijk 4, 7991 PD Dwingeloo, The Netherlands
[5] Department of Physics, McGill University, 3600 rue University, Montréal, QC H3A 2T8, Canada
[6] McGill Space Institute, McGill University, 3550 rue University, Montréal, QC H3A 2A7, Canada
[7] Jet Propulsion Laboratory, California Institute of Technology, Pasadena, CA 91109, USA
[8] Division of Physics, Mathematics, and Astronomy, California Institute of Technology, Pasadena, CA 91125, USA
[9] CSEE, West Virginia University, Morgantown, WV 26505, USA
[10] Center for Gravitational Waves and Cosmology, West Virginia University, Morgantown, WV 26505, USA
[11] Department of Physics & Astronomy, 6224 Agricultural Road, Vancouver, BC V6T 1Z1, Canada
[12] Joint Institute for VLBI ERIC, Oude Hoogeveensedijk 4, 7991 PD Dwingeloo, The Netherlands
[13] Instituto de Astronomía, Universidad Nacional Autónoma de México, Apdo. Postal 877, Ensenada, Baja California 22800, México
[14] Ioffe Institute, 26 Politekhnicheskaya st., St. Petersburg 194021, Russia
[15] Department of Space, Earth and Environment, Chalmers University of Technology, Onsala Space Observatory, SE-43992, Onsala, Sweden
[16] MIT Kavli Institute for Astrophysics and Space Research, Massachusetts Institute of Technology, 77 Massachusetts Avenue, Cambridge, MA 02139, USA
[17] Department of Physics, Massachusetts Institute of Technology, 77 Massachusetts Avenue, Cambridge, MA 02139, USA
[18] Perimeter Institute for Theoretical Physics, 31 Caroline Street N, Waterloo ON N2L 2Y5, Canada
Received 2020 April 13; revised 2020 August 18; accepted 2020 August 20; published 2020 October 6

Abstract

We report on simultaneous radio and X-ray observations of the repeating fast radio burst source FRB 180916.J0158+65 using the Canadian Hydrogen Intensity Mapping Experiment (CHIME), Effelsberg, and Deep Space Network (DSS-14 and DSS-63) radio telescopes and the Chandra X-ray Observatory. During 33 ks of Chandra observations, we detect no radio bursts in overlapping Effelsberg or Deep Space Network observations and a single burst during CHIME/FRB source transits. We detect no X-ray events in excess of the background during the Chandra observations. These non-detections imply a 5σ limit of $<5 \times 10^{-10}$ erg cm^{-2} for the 0.5–10 keV fluence of prompt emission at the time of the radio burst and 1.3×10^{-9} erg cm^{-2} at any time during the Chandra observations. Given the host-galaxy redshift of FRB 180916.J0158+65 ($z \sim 0.034$), these correspond to energy limits of $<1.6 \times 10^{45}$ erg and $<4 \times 10^{45}$ erg, respectively. We also place a 5σ limit of $<8 \times 10^{-15}$ erg s^{-1} cm^{-2} on the 0.5–10 keV absorbed flux of a persistent source at the location of FRB 180916.J0158+65. This corresponds to a luminosity limit of $<2 \times 10^{40}$ erg s^{-1}. Using an archival set of radio bursts from FRB 180916.J0158+65, we search for prompt gamma-ray emission in Fermi/GBM data but find no significant gamma-ray bursts, thereby placing a limit of 9×10^{-9} erg cm^{-2} on the 10–100 keV fluence. We also search Fermi/LAT data for periodic modulation of the gamma-ray brightness at the 16.35 days period of radio burst activity and detect no significant modulation. We compare these deep limits to the predictions of various fast radio burst models, but conclude that similar X-ray constraints on a closer fast radio burst source would be needed to strongly constrain theory.

Unified Astronomy Thesaurus concepts: Radio transient sources (2008); High energy astrophysics (739); Neutron stars (1108); X-ray bursts (1814)

1. Introduction

Fast radio bursts (FRBs) are a new class of radio transient with unknown origins (see Cordes & Chatterjee 2019; Petroff et al. 2019, for reviews). They are millisecond-long, bright (peak flux densities ∼0.1–10 Jy at ∼1 GHz) bursts and have been observed at frequencies from 300 MHz (Chawla et al. 2020) to 8 GHz (Gajjar et al. 2018). Their distances, both based on their dispersion measure (DM) excesses (in comparison to the expected Milky Way contributions; Cordes & Lazio 2002; Yao et al. 2017) and measured host-galaxy redshifts for a few sources (Chatterjee et al. 2017; Bannister et al. 2019; Ravi et al. 2019; Prochaska et al. 2019; Marcote et al. 2020), are extragalactic, and the most distant sources appear to come from cosmological distances (i.e., $z \gtrsim 0.5$; Thornton et al. 2013). The extreme luminosities and short duration of FRBs point to coherent emission originating from a compact object. Prior to the discovery of repeat bursts from some FRB sources, most models invoked cataclysmic phenomena to explain the extreme energetics of FRBs (for a catalog of models, see Platts et al. 2018). However, since the discovery of repeat bursts from FRB 121102 (Spitler et al. 2016), models that can account for

[19] NDSEG Research Fellow.
[20] NSF Graduate Research Fellow.

repetition have become increasingly the focus of theoretical work.

One central engine in particular has garnered a lot of attention: the millisecond magnetar. In this model, an FRB is powered by a young, recently formed millisecond magnetar (e.g., Lyubarsky 2014; Beloborodov 2017; Metzger et al. 2017) and may be associated with short duration or persistent emission in X-rays or gamma-rays. The older, much less energetic, magnetars in our Galaxy are known to power X-ray and gamma-ray bursts and flares on timescales of milliseconds to seconds (see Kaspi & Beloborodov 2017, for a review), which are similar to the duration of FRBs. The high-energy burst emission of magnetars comes in at least two classes: giant flares and short X-ray bursts. To date, only three magnetar giant flares have been detected in our Galaxy and the Magellanic Clouds (Evans et al. 1980; Hurley et al. 1999, 2005) with X-ray peak luminosities in the range $\sim 10^{44}$–10^{47} erg s^{-1}. Short X-ray bursts from magnetars are emitted much more frequently but are much fainter than giant flares (peak X-ray luminosities of $\sim 10^{36} - 10^{43}$ erg s^{-1}; e.g., Göğüş et al. 1999, 2000; Scholz & Kaspi 2011).

Scholz et al. (2017) undertook several campaigns of coordinated X-ray and radio observations of FRB 121102, to probe for coincident high-energy emission during the radio bursts. With these observations, upper limits were placed on X-ray (0.5–10 keV) and gamma-ray (10–100 keV) emission at the time of radio bursts. Owing to the relatively large distance to FRB 121102 ($z \sim 0.193$; luminosity distance of 972 Mpc; Tendulkar et al. 2017), these limits were found to be $\sim 10\times$ above what is expected for a magnetar giant flare (Scholz et al. 2017).

The recent success of the CHIME/FRB Collaboration in discovering repeating FRBs has led to several sources that could be much closer than FRB 121102, based on their low DM excesses (CHIME/FRB Collaboration et al. 2019). One of these sources, FRB 180916.J0158+65, was subsequently localized with milliarcsecond precision to a spiral galaxy at $z = 0.0337 \pm 0.0002$ (luminosity distance of 149 Mpc) using observations from the European VLBI Network (EVN; Marcote et al. 2020). Recently, a 16.35 days periodicity in the burst activity of FRB 180916.J0158+65 was found, where the source seems to be active in a ~5 day window (CHIME/FRB Collaboration et al. 2020), although an aliased, shorter period cannot presently be excluded. Armed with this localization, and knowledge of the periodic activity level, we were able to perform a deep, targeted, search for X-ray emission using the Chandra X-ray Observatory coordinated with radio observations at times when the detection of radio bursts from the source were highly probable. The greater proximity of FRB 180916.J0158+65 compared to FRB 121102 allows us to probe $\sim 40\times$ deeper in energy for such emission. Previously, limits have been placed on the high-energy emission of FRB 180916.J0158+65 during its active phases using INTEGRAL (Panessa et al. 2020), Swift/XRT (Tavani et al. 2020a), and Chandra (Kong et al. 2020).[21] Other studies have also placed limits on the gamma-ray emission of a large sample of FRB sources (e.g., Tendulkar et al. 2016; Cunningham et al. 2019).

Here we present simultaneous deep X-ray and radio observations on 2019 December 3 and 18 performed with the goal of detecting or constraining any X-ray counterparts to the radio bursts from FRB 180916.J0158+65. Using a larger archival set of radio burst times, we also present a search for gamma-ray emission at the times of radio bursts from FRB 180916.J0158+65. We describe the Chandra (X-ray), Fermi (gamma-ray), Effelsberg, Deep Space Network, and CHIME (radio) observations in Section 2. In Section 3 we present the results of our search for bursts in the radio observations as well as X-ray (Chandra) and gamma-ray (Fermi) emission both at the time of radio bursts and at any time during the high-energy observations. We discuss the significance of these results in Section 4.

2. Observations

2.1. Chandra X-Ray Observatory

FRB 180916.J0158+65 was observed by Chandra on 2019 December 3 (ObsID 23081) and 2019 December 18 (ObsID 23082) at epochs consistent with the "on-phase" of the periodic activity of FRB 180916.J0158+65 identified by CHIME/FRB Collaboration et al. (2020). The ACIS-S3 detector was operated in VFAINT mode with a 1/8 sub-array read out providing a $8' \times 1'$ field of view and a 0.4-s frame time. The exposure times were both ~16 ks, as listed in Table 1. Figure 1 shows a timeline of the Chandra observations and how they overlap with radio observations.

The resulting data were analyzed using CIAO[22] version 4.12 (Fruscione et al. 2006) following standard procedures recommended by the Chandra X-ray Center. Source events were extracted from a 1″-radius region (95% encircled energy) centered on the position of FRB 180916.J0158+65 and arrival times were corrected to the Solar-System Barycenter using the source position measured by Marcote et al. (2020) to a precision of ~2 milliarcseconds with the EVN.

2.2. CHIME/FRB

The CHIME/FRB backend continuously searches total intensity, polarization-summed time series from each of the 1024 beams formed across CHIME's $2^\circ \times 120^\circ$ field of view. The time series have a 0.98304-ms time resolution and 16,384 frequency channels across the 400–800 MHz band. The backend uses real-time radio-frequency interference (RFI) mitigation and a tree dedispersion algorithm to search over a wide range of trial DMs. Dispersed signals with integrated S/N values greater than the system's configurable threshold are forwarded to a post-detection pipeline to classify sources as RFI, known Galactic sources, or unknown Galactic or extragalactic signals (by comparing to predicted Galactic foreground contributions to DM). Signals are classified as FRBs (i.e., unknown extragalactic) if they are not associated with any known Galactic sources, and their observed DMs exceed the maximum values predicted by Galactic DM models (Cordes & Lazio 2002; Yao et al. 2017). See CHIME/FRB Collaboration et al. (2018) for a detailed description of the CHIME/FRB system.

On 2019 December 3, CHIME was offline for upgrades and so was unable to search for bursts at that time. On 2019 December 18, FRB 180916.J0158+65 was within the FWHM (at 600 MHz) of the CHIME/FRB beams for 14.7 min (see

[21] Based on the same Chandra observations presented here.

[22] Chandra Interactive Analysis of Observations. http://cxc.harvard.edu/ciao/.

Table 1
Summary of Joint X-Ray/Radio Observations

Telescope	ObsID/ Frequency (MHz)	Start time (UTC)	End time (UTC)	Exposure time (s)
Chandra	23081	2019 Dec 03 01:33:03	2019 Dec 03 07:01:53	16390
	23082	2019 Dec 18 03:47:29	2019 Dec 18 09:13:36	16300
CHIME/FRB[a]	400–800	2019 Dec 18 04:06:36	2019 Dec 18 04:21:22	886
Effelsberg	1210–1510	2019 Dec 2 23:29:27	2019 Dec 3 07:29:27	28800
		2019 Dec 18 02:21:17	2019 Dec 18 09:21:17	25200
DSS-14	1360–1720	2019 Dec 2 05:37:29	2019 Dec 2 07:01:29	5040
		2019 Dec 2 07:09:03	2019 Dec 2 07:50:17	2474
		2019 Dec 18 02:22:05	2019 Dec 18 03:51:05	5340
		2019 Dec 18 04:01:13	2019 Dec 18 05:35:13	5640
		2019 Dec 18 06:05:43	2019 Dec 18 07:22:43	4620
		2019 Dec 18 07:30:17	2019 Dec 18 09:04:17	5640
		2019 Dec 18 09:11:47	2019 Dec 18 10:45:47	5640
		2019 Dec 18 10:53:33	2019 Dec 18 12:18:33	5100
DSS-63	2200–2310 and 8180–8575	2019 Dec 2 02:10:35	2019 Dec 2 03:49:35	5940
		2019 Dec 2 22:58:41	2019 Dec 03 00:37:41	5940
		2019 Dec 3 02:32:47	2019 Dec 3 03:43:30	4243
		2019 Dec 18 20:53:49	2019 Dec 18 22:27:49	5640
	2205–2310 and 8180–8575	2019 Dec 18 22:36:31	2019 Dec 19 00:10:31	5640
		2019 Dec 19 00:18:27	2019 Dec 19 01:52:27	5640
		2019 Dec 19 02:00:35	2019 Dec 19 03:43:15	6160

Note.
[a] Start, end, and exposure times based on time spent by source within the 600 MHz FWHM of the CHIME/FRB formed beams.

Table 1). During that period, the source moved through the four columns of synthesized beams. As such, the sensitivity to FRB 180916.J0158+65 varied significantly over the course of the transit.

2.3. Effelsberg Radio Telescope

The Effelsberg 100-m radio telescope observed FRB 180916.J0158+65 with the 7-beam receiver (P217mm) at a center frequency of 1.36 GHz. The central beam was pointed at the precise position measured by the EVN localization (Marcote et al. 2020). These observations spanned the full extent of the Chandra observations (see Figure 1) and their start times, end times, and total on-source time are given in Table 1. The PFFTS digital backend recorded total intensity spectral data with a time resolution of 54.6 μs, 512 frequency channels, and a bandwidth of 300 MHz ($\Delta\nu = 0.586$ MHz). Before processing, the PFFTS data were converted from 32-bit floats to 8-bit unsigned integers in `sigproc` filterbank format.

The data were searched using the `PRESTO` search software (Ransom 2011).[23] Broadband, impulsive RFI was removed by identifying statistical outliers within a user-specific block of time. First, each frequency channel was rescaled using the standard deviation and median of that channel, and then the zero-DM time series was calculated. Time samples in this time series that were above the S/N threshold were considered likely to be RFI contaminated. All of the frequency channels associated with the contaminated samples were replaced by Gaussian noise with the statistics of that channel. The cleaned filterbank was then passed to `rfifind` for further RFI excision. The data were then downsampled by a factor of eight in time and dedispersed with 100 trial DMs ranging from 300 pc cm^{-3} to 400 pc cm^{-3} (FRB 180916.J0158+65 has a DM of 349 pc cm^{-3}; CHIME/FRB Collaboration et al. 2019) in steps of 1 pc cm^{-3} with `prepsubband`. Each time series was convolved with a template bank of boxcar matched filters yielding effective time resolutions of 0.44 ms to 17.5 ms, and candidate bursts were identified in each time series by applying a detection threshold of S/N > 6 (`single_pulse_search.py`). The results were inspected by eye, and promising candidates were further investigated by looking at a time-frequency snapshot around each candidate.

2.4. Deep Space Network

The Deep Space Network (DSN) observed FRB 180916.J0158+65 for a total of ~22 hr, partially overlapping with the Chandra observations (see Figure 1), using DSS-14 and DSS-63, two 70-m diameter radio antennas located in Goldstone, California and Robledo, Spain. FRB 180916.J0158+65 was observed at *L*-band (center frequency of 1.5 GHz; data recorded in left circular polarization) using DSS-14 for a total of 11 hr over eight separate scans. DSS-63 observed FRB 180916.J0158+65 simultaneously at *S*-band (center frequency of 2.3 GHz) and *X*-band (center frequency of 8.4 GHz) with data recorded in both left and right circular polarization for a total of 11 hr in seven separate scans (see Table 1). The *L*-band system on DSS-14 spans roughly 500 MHz of bandwidth, but only 250 MHz of the total bandwidth was usable during our observations after RFI mitigation. At *S*-band, the first three DSS-63 observations were recorded with a bandwidth of 110 MHz and the last four observations were recorded with 105 MHz. The *X*-band data were recorded with a bandwidth of 395 MHz.

Data were recorded using pulsar backends that record channelized power spectral density measurements in filterbank

[23] https://github.com/scottransom/presto

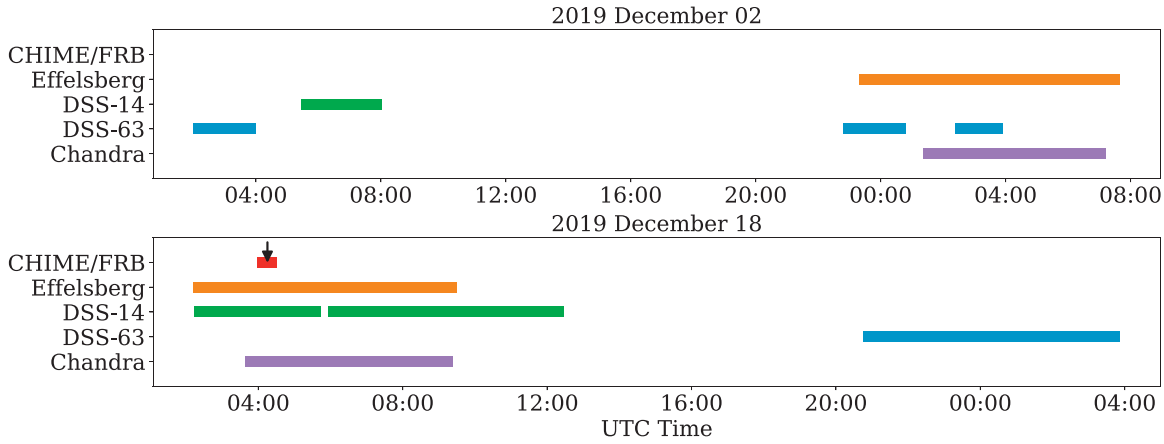

Figure 1. Timeline of Chandra observations (purple) and the coordinated radio observations from CHIME/FRB (red), Effelsberg (orange), and the Deep Space Network (DSS-14, in green, and DSS-63, in blue, respectively). The bars show the times when each telescope was observing FRB 180916.J0158+65. The arrow on 2019 December 18 marks the time of the CHIME/FRB-detected burst.

format. The *L*-band data were recorded with a time and frequency resolution of 102.4 μs and 0.625 MHz, respectively. The *S*-band and *X*-band data were recorded with a time and frequency resolution of 2.2 ms and 0.464 MHz, respectively. We performed short observations of a bright pulsar (PSR B0329+54) at various times throughout the observing campaign to validate the quality of the data. The data were flux calibrated by measuring the $T_{\rm sys}$ at each frequency band while the antenna was in the stow position. We then corrected the $T_{\rm sys}$ values for elevation effects, which were minimal since all of our observations occurred when the source elevation was above 20°.

The data processing procedures followed those described in previous DSN studies of pulsars (e.g., Majid et al. 2017; Pearlman et al. 2018, 2019). In each data set, we corrected for the bandpass slope across the frequency band. Bad frequency channels corrupted by RFI were identified using the PSRCHIVE software (Hotan et al. 2004) and masked. We also subtracted the moving average from each data point using 0.5 s around each time sample in order to remove any long timescale temporal variability. The cleaned data from each epoch were then dedispersed with trial DMs between 300 and 400 pc cm^{-3} with trial spacings of 2 pc cm^{-3} at *L*-band, 5 pc cm^{-3} at *S*-band, and 50 pc cm^{-3} at *X*-band. We searched for FRBs using a matched filtering algorithm, where each dedispersed time-series was convolved with logarithmically spaced boxcar functions with widths ranging between 1–300 times the native time resolution. FRB candidates with detection S/N > 6 were saved and classified using a GPU-accelerated machine-learning pipeline based on the FETCH (Fast Extragalactic Transient Candidate Hunter) package (Agarwal et al. 2020).

2.5. Fermi Gamma-Ray Space Telescope

The Fermi telescope has two sets of detectors on board, the Gamma-ray Burst Monitor (GBM; Meegan et al. 2009) and the Large Area Telescope (LAT; Atwood et al. 2009). The GBM consists of 12 sodium iodide (NaI; 8 keV–40 MeV) and 2 bismuth germanate (BGO; 300 keV–40 MeV) scintillators pointed in various directions to provide all-sky coverage to gamma-rays. In this work we use only the NaI detectors. The GBM instrument records data in several different data products, but here we use only the time-tagged events (TTE) data which provides event data with 2-μs time resolution and 128 energy channels. The LAT is a pair-conversion telescope providing sensitivity to gamma-ray photons in the range 20 MeV–300 GeV in a 2.4 sr (20% of sky) field of view. The LAT images the sky with a time resolution of 10 μs or better. The LAT collaboration periodically releases improved reprocessing of their gamma-ray events. Here we use the most recent release, Pass 8.

3. Analysis and Results

3.1. Radio Bursts

During the 2019 December 18 transit of FRB 180916.J0158+65 over CHIME, which was simultaneous with a Chandra observation, a single radio burst was detected by CHIME/FRB. The burst was detected at MJD 58835.17721035 (barycentric after correcting for dispersive delay), 446 s after the start of the Chandra observation, with a band-averaged S/N of 12.8 which corresponds to a peak flux density of 0.4 ± 0.2 Jy and fluence of 2.9 ± 0.7 Jy ms (see CHIME/FRB Collaboration et al. 2020, for additional details on this burst).

In the simultaneous Effelsberg observations, no bursts with S/N > 6 were identified by the PRESTO search. Assuming a system equivalent flux density of 20 Jy for the P217mm receiver and S/N > 6, the fluence threshold is 0.15 Jy ms $\sqrt{(w/1\ \mathrm{ms})}$, where w is the burst duration in ms. The Effelsberg time series were also manually inspected around the time of detected CHIME/FRB bursts and no excess was found. In the DSN observations listed in Table 1, no radio bursts were detected. For a pulse width of w, the average fluence thresholds (for S/N > 6) on the peak flux densities during these epochs are: 0.29 Jy ms $\sqrt{(w/1\ \mathrm{ms})}$ at *L*-band, 0.25 Jy ms $\sqrt{(w/1\ \mathrm{ms})}$ at *S*-band, 0.14 Jy ms $\sqrt{(w/1\ \mathrm{ms})}$ at *X*-band.

3.2. Limits on Prompt X-Ray Emission

We searched the Chandra observations both for X-ray photons arriving nearby in time to the CHIME/FRB-detected radio burst and at any time during the observations. In the 2019 December 3 Chandra observation, a single photon was detected at the source position, but there were no detected radio bursts in overlapping radio observations. In the 2019 December 18

Table 2
Burst Limits from Chandra for Different X-Ray Spectral Models

Model	N_H (cm^{-2})	kT/Γ (keV/-)	Absorbed 0.5–10 keV Fluence Limit (10^{-11} erg cm^{-2})	Unabsorbed 0.5–10 keV Energy Limit[a] (10^{45} erg)	Extrapolated 10 keV–1 MeV Energy Limit[a] (10^{47} erg)
Blackbody	10^{22}	10	90	3	0.7
Blackbody	10^{24}	10	200	20	7[b]
Cutoff PL	10^{22}	0.5	50	1.4	5
Cutoff PL	10^{24}	0.5	180	20	90[b]
Soft PL	10^{22}	2	20	0.9	0.014
Soft PL	10^{24}	2	120	50	0.8

Notes. 5σ confidence upper limits. See Section 3.2 for details.
[a] Assuming the measured luminosity distance to FRB 180916.J0158+65, 149 Mpc (Marcote et al. 2020).
[b] More stringent limits on these models are available from Fermi/GBM. See Section 3.4.

Chandra observation, a single photon was detected at the source position, 4.7 hr after the CHIME/FRB-detected radio burst and 500 s before the end of the Chandra observation. We take into account the dispersion delay of the radio bursts (9 s at 400 MHz) when comparing to the times of high-energy photons. The background count rate in the source extraction regionduring the observation was 6×10^{-5} counts s^{-1}. This leads to a probability of 64% of detecting one or more photons within 4.7 hr of the radio burst. Given this high false alarm probability, we have no reason to associate the detection with FRB 180916.J0158+65. For both observations, the detection of a single X-ray count within the source extraction region of FRB 180916.J0158+65 is consistent with the background count rate.

Following Scholz et al. (2017), we place upper limits using Poisson statistics and the Bayesian method of Kraft et al. (1991). For all limits in this work, we use a stringent confidence level of 0.9999994, the equivalent of the 5σ width of a Gaussian distribution. For brevity, we refer to this confidence level as "5σ" below. We first derive a "model-independent" limit, that is, assuming an equal probability of a source photon occurring across the 0.5–10 keV band (note that this is effectively assuming a flat spectral model with zero X-ray absorption; see below for exploration of more reasonable models). This 5σ confidence upper limit on the 0.5–10 keV fluence for a single X-ray burst at the time of the detected radio bursts is 5×10^{-10} erg cm^{-2} corresponding to 1.6×10^{45} erg at the luminosity distance of FRB 180916.J0158+65. These fluence and energy limits are valid for any burst duration contained within 446 s before the radio bursts (i.e., from the beginning of the observation) and 4.7 hr after (i.e., up to the time of the Chandra background photon). The fluence limit for an X-ray burst arriving at any other time during the Chandra observations is 1.3×10^{-9} erg cm^{-2} for an assumed duration of 5 ms, corresponding to an energy limit of 4×10^{45} erg.

As discussed in Scholz et al. (2017), the implied limit on the emitted energy of a putative X-ray burst depends strongly on the underlying spectral model of the burst. By assuming a spectral model and taking into account the spectral response of Chandra, a fluence limit for that underlying spectral model can be calculated. To generate the assumed source spectra we used XSPEC v12.10.1f with abundances from Wilms et al. (2000) and photoelectric cross-sections from Verner et al. (1996). In order to enable direct comparison, we assume the same fiducial models used by Scholz et al. (2017) for FRB 121102: a blackbody spectrum with $kT = 10$ keV as observed in magnetar hard X-ray bursts (e.g., Lin et al. 2012; An et al. 2014), a cutoff power law with index $\Gamma = 0.5$ and cutoff energy of 500 keV, similar to a SGR 1806−20-like giant flare spectrum (Mazets et al. 2005; Palmer et al. 2005) and a power-law model with index $\Gamma = 2$ as an example soft spectrum, a contrast to the hard magnetar burst models. In Table 2 we show the resulting fluence and energy limits assuming these source models. For X-ray absorption, we assume two values, 10^{22} cm^{-2} and 10^{24} cm^{-2}. The first is a typical value for a sightline passing through the Milky Way and the disk of a Milky-Way-like host galaxy and the second is an extreme value to show the effects of a high degree of absorption from material close to the source (such as the surrounding supernova ejecta in the magnetar model; Metzger et al. 2017).

3.3. Limits on Persistent X-Ray Emission

To place the best-possible limits on a persistent source we combined the two Chandra observations for a total of 33 ks of exposure time. In these two observations, only two events were detected in a 1″-radius region centered on the position of FRB 180916.J0158+65. We measure a 0.5–10 keV background count rate in a 25″-radius region chosen to be away from the source of 0.7 counts s^{-1} sq. $arcsec^{-2}$. Given this background rate, the two detected counts are consistent with the background in the combined observations. Using these detected and measured background rates, we measure a 5σ count rate limit of 5.5×10^{-4} counts s^{-1}, using the Bayesian method of Kraft et al. (1991). Assuming a photoelectrically absorbed power-law source spectrum with $\Gamma = 2$ and $N_H \sim 1 \times 10^{22}$ cm^{-2}, the 5σ upper limit on the persistent 0.5–10 keV X-ray absorbed flux from FRB 180916.J0158+65 or its host galaxy is 8×10^{-15} erg cm^{-2} s^{-1}. At the luminosity distance of FRB 180916.J0158+65 this corresponds to an isotropic luminosity limit of 2×10^{40} erg s^{-1}.

3.4. Limits on Prompt Gamma-Ray Emission

We searched data from the Fermi/GBM for gamma-ray counterparts at the time of radio bursts from FRB 180916.J0158+65 using a similar analysis to that in Scholz et al. (2017). We searched the TTE GBM data in the energy range 10–100 keV for NaI detectors that were pointed <60° from the source position. The 2018 December 18 bursts in this work were not visible to GBM as the source was occulted by the Earth at the time. However, of the 28 bursts in CHIME/FRB Collaboration et al. (2020), 12 bursts occurred at a time when TTE data were available and the source was <60° from at least one NaI detector and not occulted by the Earth. For these

bursts, we searched each TTE time series for excess counts in 1 and 5 ms bins in a 20 s window centered on the arrival time of the CHIME/FRB-detected radio burst (after correcting for the dispersive delay). We find no signals that are not attributable to Poisson fluctuations from the background count rate at a 5σ confidence level. Taking into account the effective area of the NaI detectors[24] toward the source position at the time of each event, the background count rate, the number of trials searched in each 20 s window, and assuming a burst timescale of 0.1 s, we find upper limits in the range $3–7 \times 10^{-8}$ erg cm^{-2} on the 10–100 keV fluence of each burst. These correspond to a 10–100 keV burst isotropic energy limits in the range $8 \times 10^{46}–2 \times 10^{47}$ erg at the measured luminosity distance of FRB 180916.J0158+65. If we assume a burst of gamma-rays is emitted at the time of each radio burst, and thus consider the product of the posterior probability distributions of the fluence of each burst, the 5σ 10–100 keV fluence limit becomes 9×10^{-9} erg cm^{-2}. At the measured luminosity distance of FRB 180916.J0158+65, this corresponds to a 10–100 keV burst energy limit of 3×10^{46} erg. These limits are more constraining than the extrapolated limits for prompt emission from the Chandra observations presented in Table 2 for the highly absorbed hard (10 keV blackbody and cutoff power-law) models. For those fiducial models the 10 keV to 1 MeV energy limits are 1×10^{47} erg and 2×10^{48} erg, respectively. No bursts from this work or CHIME/FRB Collaboration et al. (2020) occurred in the Fermi/LAT field of view.

3.5. Search for Periodic Gamma-Ray Emission

All Fermi/LAT photons with energies above 1 GeV and within a 5° radius region around the coordinates of the source were selected, conservatively reflecting the ∼3° 95% containment radius for the point-spread function at 1 GeV. We then filtered the data based on event class and zenith angle to ensure data quality and exclude Earth-limb photons. Each of the remaining photons was then assigned a weight according to its distance from the source based on an empirical approximation to the LAT PSF described in (Bruel 2019). We correct for exposure in each phase bin before performing a weighted H-test on the resultant pulse profile as described in (Kerr 2011). These data spans all 11 yr from MJD 54683 to MJD 58907. However, we also perform the H-test on the data restricted only to the last 5 yr as well as restricted only to after the source was first detected by CHIME/FRB (MJD 58377). We repeat this analysis method for eight potential aliased frequencies, f_N, for $N \leqslant 4$ in $f_N = Nf_{\rm sid} \pm f_0$; (where $f_{\rm sid}$ is the frequency of a sidereal day and $f_0 = (16.35\ {\rm days})^{-1}$; see CHIME/FRB Collaboration et al. 2020) and for each time span. In the 27 combinations we find no single-trial false alarm probability lower than 1%, except for in the case of $N = -3$ which had a significance of approximately 3σ (single-trial false alarm probability 0.08%) in the 11 yr sample. We attribute this to random noise given the 27 trial periods searched. Further, in the truncated data sets, since initial CHIME/FRB detection and in the last 5 yr, we find a false alarm probability of 16.7% and 32.4% respectively for the $N = -3$ case.

[24] Generated using the GBM Response Generator https://fermi.gsfc.nasa.gov/ssc/data/analysis/rmfit/DOCUMENTATION.html.

4. Discussion

4.1. Comparison to Previous Limits

The limits determined here can be compared to the similar campaign performed for FRB 121102 using XMM-Newton and Chandra observations that were simultaneous with radio observations (Scholz et al. 2017). Figure 2 shows the limits, in burst energy, as a function of photon energy for both FRB 121102, from Scholz et al. (2017), and FRB 180916.J0158+65, from this work. As FRB 180916.J0158+65 is 6.5 times closer than FRB 121102, the single-burst energy limits from Chandra ACIS and Fermi GBM observations are ∼40× more constraining. However, the campaign on FRB 121102 included several Chandra and XMM-Newton observations during which 11 radio bursts were detected, compared to the single burst detected for FRB 180916.J0158+65 in this work. This means that the (flat-model) single-burst 0.5–10 keV energy limit for prompt emission from FRB 180916.J0158+65, 1.6×10^{45} erg, is only ∼3× more constraining than the combined limit for FRB 121102, 4×10^{45} erg, which was derived under the assumption that an X-ray burst of similar fluence was emitted near the time of each radio burst.

The $N_{\rm H}$ values assumed in the above calculations are the same as those taken for FRB 121102 (Scholz et al. 2017), but may not be applicable for FRB 180916.J0158+65. From the DM budget presented by Marcote et al. (2020) and the DM–$N_{\rm H}$ relation from He et al. (2013), we can estimate what the $N_{\rm H}$ toward FRB 180916.J0158+65 could be. The total DM measured for FRB 180916.J0158+65 is 349 pc cm^{-3}. Assuming the intergalactic medium (IGM) does not contribute significantly to $N_{\rm H}$, we subtract the IGM contribution to the DM, determined from the DM–z relation (Inoue 2004), 34 pc cm^{-3}. This leaves a Milky Way plus host DM of 291 pc cm^{-3}, which from the DM–$N_{\rm H}$ relation roughly corresponds to $N_{\rm H} = 10^{22}$ cm^{-2}, as used above. The high $N_{\rm H}$ value, 10^{24} cm^{-2}, was used in Scholz et al. (2017) to simulate extreme X-ray absorption local to the source due to a high ratio of atomic metals to free electrons, which could occur in a decades-old supernova remnant (Metzger et al. 2017). However, Chawla et al. (2020) argues against such a young remnant for FRB 180916.J0158+65 because of their recent detection of FRB 180916.J0158+65 at 300 MHz. This detection limits the size, and thus age, of a remnant due to the requirement that the environment is optically thin to free–free absorption at 300 MHz. As such, we consider this highly absorbed scenario unlikely for FRB 180916.J0158+65, though still consider it here for comparison to past limits on FRB 121102.

Our burst limits can be compared to those placed for FRB 180916.J0158+65 using other telescopes. Tavani et al. (2020a) place a 3σ persistent 0.3–10 keV X-ray flux of 5.5×10^{-14} erg s^{-1} cm^{-2} using 10 ks of Swift/XRT observations during active periods of FRB 180916.J0158+65. For our corresponding limit we use a more stringent 5σ confidence interval. Our 3σ limit, however, would be 4×10^{-15} erg s^{-1} cm^{-2}, just over an order of magnitude deeper than the Swift/XRT limit. Using INTEGRAL/IBIS, Panessa et al. (2020) place 3σ upper limits on the 28–80 keV gamma-ray flux of 3.4×10^{-8} erg s^{-1} cm^{-2} for 100-ms-long bursts at any time during the INTEGRAL observations. This is very similar to the 10–100 keV Fermi/GBM limit placed here on gamma-ray emission at the time of radio bursts (translated to a 3σ limit on flux it is 7×10^{-8} erg s^{-1} cm^{-2}).

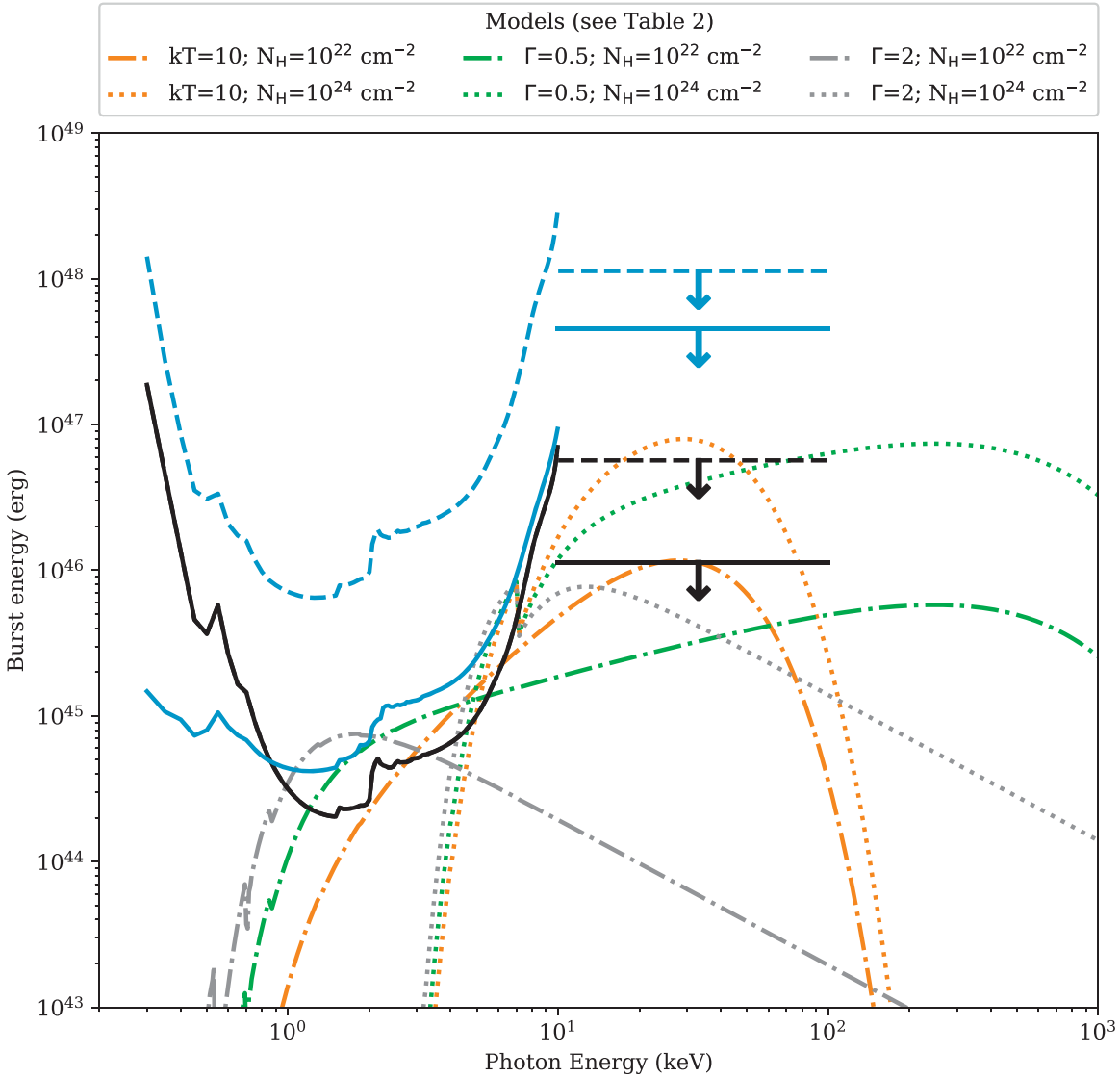

Figure 2. Limits on the energy of X-ray and gamma-ray bursts at the time of radio bursts from FRB 180916.J0158+65 (in black; this work) and FRB 121102 (in blue; from Scholz et al. 2017). The limits in the 0.5–10 keV range are from Chandra, and in the 10–100 keV range are from Fermi/GBM. Dashed and solid lines show the 5σ upper limits as a function of X-ray photon energy, at the time of a single radio burst and stacking those limits (see Section 4.1), respectively. The dotted–dashed lines show different burst spectra that are photoelectrically absorbed, assuming $N_{\rm H} = 10^{22}$ cm^{-2}, plotted at their 0.5–10 keV fluence limits that result from a stacked search of the times of the radio bursts. The dotted lines show the same spectral models but with $N_{\rm H} = 10^{24}$ cm^{-2} to show the effects of possible heavy absorption local to the source. Orange lines represent a blackbody model with $kT = 10$ keV, green curves shows a cutoff power-law model with $\Gamma = 0.5$ and $E_{\rm cut} = 500$ keV, and the gray curves show a soft power law with $\Gamma = 2$ in order to illustrate how different underlying spectra affect the interpretation of the X-ray observations.

4.2. Comparison to FRB Models

We can compare our X-ray and gamma-ray energy limits to the energy emitted by the 2004 giant flare of SGR 1806−20, the most energetic event detected from a Galactic magnetar. Though most interesting in the context of the magnetar model, this event is the most luminous transient event yet detected in our Galaxy, so is therefore interesting in a model-agnostic context as well. The bright onset of the flare had a spectrum similar to that of our canonical giant flare model, an isotropic gamma-ray luminosity of $\sim 10^{47}$ erg s^{-1} (measured in the ∼20 keV–10 MeV band; Mazets et al. 2005; Palmer et al. 2005), and a duration of ∼100 ms. This gives an emitted energy in a 10 keV–1 MeV band of $\sim 10^{46}$ erg. Our gamma-ray extrapolated isotropic energy limit for the giant-flare-like cutoff power-law model in Table 2 is still an order of magnitude higher than this energy emitted by SGR 1806−20. Further, Galactic magnetar activity includes much fainter events. The giant flares from magnetars SGR 0526−66 and SGR 1900+14 had peak luminosities of $10^{44\text{-}45}$ erg s^{-1}, over 100× lower than the SGR 1806−20 giant flare. Short X-ray bursts from magnetars span far fainter luminosities ($\sim 10^{36} - 10^{43}$ erg s^{-1}; e.g., Göğüş et al. 1999, 2000; Scholz & Kaspi 2011).

For the synchrotron blast wave model of FRBs, Metzger et al. (2019) and Margalit et al. (2020) predict an expected maximum fluence for a gamma-ray flare of $\sim 10^{-13} - 10^{-12}$ erg cm^{-2} for FRB 180916.J0158+65. This is far below the detection threshold of either our extrapolated X-ray limits (which would depend heavily on what the spectrum of the gamma-ray flare would be in the soft X-ray band) or our Fermi limits. The above shows that although the distance to FRB 180916.J0158+65 is low for an FRB, it is still much too distant to probe the energies expected for magnetar-like activity.

The discovery of a 16.35 days periodicity in the radio burst activity of FRB 180916.J0158+65 (CHIME/FRB Collaboration et al. 2020) has recently led to models in which the source —still in many models a neutron star—is in an orbit or precessing. However, the current models do not clearly predict X-ray or gamma-ray emission that would be detectable using current instruments, given the distance to FRB 180916.J0158 +65. For example, Mottez et al. (2020) describe a situation in which the relativistic wind of a pulsar or magnetar impinges on an orbiting planetary companion, creating an Alfvén wing that if viewed downstream could be a source of FRBs. Given that this scenario does not require powerful flares from the neutron star itself, observable X-ray emission at the distance of FRB 180916.J0158+65 is not expected. Ioka & Zhang (2020) present a binary "comb" model in which FRBs are produced when the magnetosphere of a neutron star interacts with the wind of a massive stellar companion, but make no specific predictions for the brightness of high-energy emission. Levin et al. (2020) note that a hyper-active magnetar that is driven by fast ambipolar diffusion in the core is expected to precess freely with a period of hours to weeks. This could explain the periodicity of observed burst activity, but there is no reason to think that the magnetar flares themselves would be intrinsically brighter or dimmer compared to those we have considered above.

Persistent X-ray emission from FRB sources could arise from a pulsar wind nebula (if the FRB source is a rotation or magnetically powered pulsar). We therefore compare our limit to the X-ray luminosity of the Crab Nebula, 10^{37} erg s^{-1}. This is three orders-of-magnitude lower than our persistent X-ray luminosity limit of 2×10^{40} erg s^{-1}. We can also compare our X-ray luminosity limit to the luminosities of the brightest X-ray sources. It is comparable to the luminosities of low-luminosity active galactic nuclei (Terashima & Wilson 2003), bright high-mass X-ray binaries (Sazonov & Khabibullin 2017), and ultraluminous X-ray sources (Earnshaw et al. 2019). For all of these sources, their luminosity distributions extend well below our limit so we cannot rule out any such association with the source of FRB 180916.J0158+65. However, it shows that future observations of FRBs closer than FRB 180916.J0158 +65 have the potential to make a detection if any of these objects are associated with the source.

Note that when translating our flux and fluence limits here to limits on luminosity or energy, we assume an isotropic energy release. If the high-energy emission from an FRB source is beamed, the energy emitted would of course be lower as its emitted over a narrower solid angle.

For both prompt and persistent emission, we are only just beginning to probe the brightest of possible counterparts to repeating FRBs. Even for the closest sources, say at <100 Mpc, ruling out high-energy activity from most models, such as that expected from a magnetar, is challenging. It is, however, important to place the most stringent possible limits for closer sources, in case there are much more energetic counterparts to repeating FRBs.

Late in the preparation of this work, we became aware of the works of Pilia et al. (2020) and Tavani et al. (2020b) where limits were placed on the high-energy emission of FRB 180916.J0158+65 during its active phases using XMM-Newton, Swift/XRT, and AGILE. The deep XMM-Newton limits placed on the X-ray emission by Pilia et al. (2020) at the time of radio bursts using are similar to ours placed here with Chandra. The AGILE limits probe a higher energy range than we considered here with Fermi/GBM. The persistent X-ray emission limits from Swift (Tavani et al. 2020b) and XMM-Newton (Pilia et al. 2020) are consistent with those we place here.

We thank the Dominion Radio Astrophysical Observatory, operated by the National Research Council Canada, for gracious hospitality and useful expertise. The CHIME/FRB Project is funded by a grant from the Canada Foundation for Innovation 2015 Innovation Fund (Project 33213), as well as by the Provinces of British Columbia and Québec, and by the Dunlap Institute for Astronomy and Astrophysics at the University of Toronto. Additional support was provided by the Canadian Institute for Advanced Research (CIFAR), McGill University and the McGill Space Institute via the Trottier Family Foundation, and the University of British Columbia. The Dunlap Institute is funded by an endowment established by the David Dunlap family and the University of Toronto. Research at Perimeter Institute is supported by the Government of Canada through Industry Canada and by the Province of Ontario through the Ministry of Research & Innovation. The National Radio Astronomy Observatory is a facility of the National Science Foundation operated under cooperative agreement by Associated Universities, Inc. This work is based on observations with the 100-m telescope of the MPIfR (Max-Planck-Institut für Radioastronomie) at Effelsberg. We thank the DSN scheduling team and the Goldstone Deep Space Communication Complex (GDSCC) and the Madrid Deep Space Communication Complex (MDSCC) staff for scheduling and carrying out the DSN observations. A portion of this research was performed at the Jet Propulsion Laboratory, California Institute of Technology and the Caltech campus, under a Research and Technology Development Grant through a contract with the National Aeronautics and Space Administration. U.S. government sponsorship is acknowledged.

A.B.P. acknowledges support by the Department of Defense (DoD) through the National Defense Science and Engineering Graduate (NDSEG) Fellowship Program and by the National Science Foundation (NSF) Graduate Research Fellowship under Grant No. DGE-1144469. B.M. acknowledges support from the Spanish Ministerio de Economía y Competitividad (MINECO) under grant AYA2016-76012-C3-1-P. D.M. is a Banting Fellow. F.K. is supported by the Swedish Research Council. FRB research at UBC is supported by an NSERC Discovery Grant and by the Canadian Institute for Advanced Research. J.W.T.H. acknowledges funding from an NWO Vici fellowship. L.G.S. is a Lise-Meitner independent research group leader and acknowledges support from the Max Planck Society. M.B. is supported by an FRQNT Doctoral Research Award. P.C. is supported by an FRQNT Doctoral Research Award. P.S. is a Dunlap Fellow and an NSERC Postdoctoral Fellow. B.M.G. acknowledges the support of the Natural Sciences and Engineering Research Council of Canada (NSERC) through grant RGPIN-2015-05948, and of the Canada Research Chairs program. V.M.K. holds the Lorne Trottier Chair in Astrophysics & Cosmology and a Distinguished James McGill Chair and receives support from an NSERC Discovery Grant and Herzberg Award, from an R. Howard Webster Foundation Fellowship from the Canadian Institute for Advanced Research (CIFAR), and from the FRQNT Centre de Recherche en Astrophysique du Québec. W.A.M, T.A.P, and C.J.N acknowledge support by the Jet

Propulsion Laboratory's Spontaneous Concept Research and Technology Development program. Z.P. is supported by a Schulich Graduate Fellowship.

ORCID iDs

P. Scholz https://orcid.org/0000-0002-7374-7119
A. Cook https://orcid.org/0000-0001-6422-8125
J. W. T. Hessels https://orcid.org/0000-0003-2317-1446
V. M. Kaspi https://orcid.org/0000-0001-9345-0307
W. A. Majid https://orcid.org/0000-0002-4694-4221
A. Naidu https://orcid.org/0000-0002-9225-9428
A. B. Pearlman https://orcid.org/0000-0002-8912-0732
L. G. Spitler https://orcid.org/0000-0002-3775-8291
K. M. Bandura https://orcid.org/0000-0003-3772-2798
M. Bhardwaj https://orcid.org/0000-0002-3615-3514
T. Cassanelli https://orcid.org/0000-0003-2047-5276
P. Chawla https://orcid.org/0000-0002-3426-7606
B. M. Gaensler https://orcid.org/0000-0002-3382-9558
D. C. Good https://orcid.org/0000-0003-1884-348X
A. Josephy https://orcid.org/0000-0003-3059-6223
R. Karuppusamy https://orcid.org/0000-0002-5307-2919
A. Keimpema https://orcid.org/0000-0002-5575-2774
A. Yu. Kirichenko https://orcid.org/0000-0002-8139-8414
F. Kirsten https://orcid.org/0000-0001-6664-8668
J. Kocz https://orcid.org/0000-0003-0249-7586
C. Leung https://orcid.org/0000-0002-4209-7408
B. Marcote https://orcid.org/0000-0001-9814-2354
K. Masui https://orcid.org/0000-0002-4279-6946
J. Mena-Parra https://orcid.org/0000-0002-0772-9326
M. Merryfield https://orcid.org/0000-0003-2095-0380
D. Michilli https://orcid.org/0000-0002-2551-7554
C. J. Naudet https://orcid.org/0000-0001-6898-0533
K. Nimmo https://orcid.org/0000-0003-0510-0740
Z. Pleunis https://orcid.org/0000-0002-4795-697X
T. A. Prince https://orcid.org/0000-0002-8850-3627
M. Rahman https://orcid.org/0000-0003-1842-6096
K. Shin https://orcid.org/0000-0002-6823-2073
I. H. Stairs https://orcid.org/0000-0001-9784-8670
S. P. Tendulkar https://orcid.org/0000-0003-2548-2926
K. Vanderlinde https://orcid.org/0000-0003-4535-9378

References

Agarwal, D., Aggarwal, K., Burke-Spolaor, S., Lorimer, D. R., & Garver-Daniels, N. 2020, MNRAS, 497, 1661
An, H., Kaspi, V. M., Beloborodov, A. M., et al. 2014, ApJ, 790, 60
Atwood, W. B., Abdo, A. A., Ackermann, M., et al. 2009, ApJ, 697, 1071
Bannister, K. W., Deller, A. T., Phillips, C., et al. 2019, Sci, 365, 565
Beloborodov, A. M. 2017, ApJL, 843, L26
Bruel, P. 2019, A&A, 622, A108
Chatterjee, S., Law, C. J., Wharton, R. S., et al. 2017, Natur, 541, 58
Chawla, P., Andersen, B. C., Bhardwaj, M., et al. 2020, ApJ, 896, 41
CHIME/FRB Collaboration, Amiri, M., Andersen, B. C., et al. 2020, Natur, 582, 351
CHIME/FRB Collaboration, Amiri, M., Bandura, K., et al. 2018, ApJ, 863, 48
CHIME/FRB Collaboration, Andersen, B. C., Bandura, K., et al. 2019, ApJL, 885, L24
Cordes, J. M., & Chatterjee, S. 2019, ARA&A, 57, 417
Cordes, J. M., & Lazio, T. J. W. 2002, arXiv:astro-ph/0207156
Cunningham, V., Cenko, S. B., Burns, E., et al. 2019, ApJ, 879, 40
Earnshaw, H. P., Roberts, T. P., Middleton, M. J., Walton, D. J., & Mateos, S. 2019, MNRAS, 483, 5554
Evans, W. D., Klebesadel, R. W., Laros, J. G., et al. 1980, ApJL, 237, L7
Fruscione, A., McDowell, J. C., Allen, G. E., et al. 2006, Proc. SPIE, 6270, 62701V
Gajjar, V., Siemion, A. P. V., Price, D. C., et al. 2018, ApJ, 863, 2
Göğüş, E., Woods, P. M., Kouveliotou, C., et al. 1999, ApJL, 526, L93
Göğüş, E., Woods, P. M., Kouveliotou, C., et al. 2000, ApJL, 532, L121
He, C., Ng, C.-Y., & Kaspi, V. 2013, ApJ, 768, 64
Hotan, A. W., van Straten, W., & Manchester, R. N. 2004, PASA, 21, 302
Hurley, K., Boggs, S. E., Smith, D. M., et al. 2005, Natur, 434, 1098
Hurley, K., Cline, T., Mazets, E., et al. 1999, Natur, 397, 41
Inoue, S. 2004, MNRAS, 348, 999
Ioka, K., & Zhang, B. 2020, ApJ, 893, 26
Kaspi, V. M., & Beloborodov, A. M. 2017, ARA&A, 55, 261
Kerr, M. 2011, ApJ, 732, 38
Kong, A. K. H., Li, K. L., Hui, C. Y., & Yu, H. F. 2020, ATel, 13589, 1
Kraft, R. P., Burrows, D. N., & Nousek, J. A. 1991, ApJ, 374, 344
Levin, Y., Beloborodov, A. M., & Bransgrove, A. 2020, ApJ, 895, 30
Lin, L., Göğüş, E., Baring, M. G., et al. 2012, ApJ, 756, 54
Lyubarsky, Y. 2014, MNRAS, 442, L9
Majid, W. A., Pearlman, A. B., Dobreva, T., et al. 2017, ApJL, 834, L2
Marcote, B., Nimmo, K., Hessels, J. W. T., et al. 2020, Natur, 577, 190
Margalit, B., Metzger, B. D., & Sironi, L. 2020, MNRAS, 494, 4627
Mazets, E. P., Cline, T. L., Aptekar, R. L., et al. 2005, arXiv:astro-ph/0502541
Meegan, C., Lichti, G., Bhat, P. N., et al. 2009, ApJ, 702, 791
Metzger, B. D., Berger, E., & Margalit, B. 2017, ApJ, 841, 14
Metzger, B. D., Margalit, B., & Sironi, L. 2019, MNRAS, 485, 4091
Mottez, F., Voisin, G., & Zarka, P. 2020, arXiv:2002.12834
Palmer, D. M., Barthelmy, S., Gehrels, N., et al. 2005, Natur, 434, 1107
Panessa, F., Savchenko, V., Ferrigno, C., Bazzano, A., & Ubertini, P. 2020, ATel, 13466, 1
Pearlman, A. B., Majid, W. A., & Prince, T. A. 2019, AdAst, 2019, 6325183
Pearlman, A. B., Majid, W. A., Prince, T. A., Kocz, J., & Horiuchi, S. 2018, ApJ, 866, 160
Petroff, E., Hessels, J. W. T., & Lorimer, D. R. 2019, A&ARv, 27, 4
Pilia, M., Burgay, M., Possenti, A., et al. 2020, ApJ, 896, 40
Platts, E., Weltman, A., Walters, A., et al. 2018, PhR, 821, 1
Prochaska, J. X., Macquart, J.-P., McQuinn, M., et al. 2019, Sci, 366, 231
Ransom, S. 2011, PRESTO: PulsaR Exploration and Search TOolkit, Astrophysics Source Code Library, ascl:1107.017
Ravi, V., Catha, M., D'Addario, L., et al. 2019, Natur, 572, 352
Sazonov, S., & Khabibullin, I. 2017, MNRAS, 466, 1019
Scholz, P., Bogdanov, S., Hessels, J. W. T., et al. 2017, ApJ, 846, 80
Scholz, P., & Kaspi, V. M. 2011, ApJ, 739, 94
Spitler, L. G., Scholz, P., Hessels, J. W. T., et al. 2016, Natur, 531, 202
Tavani, M., Verrecchia, F., Casentini, C., et al. 2020a, ATel, 13462, 1
Tavani, M., Verrecchia, F., Casentini, C., et al. 2020b, ApJ, 893, 42
Tendulkar, S. P., Bassa, C. G., Cordes, J. M., et al. 2017, ApJL, 834, L7
Tendulkar, S. P., Kaspi, V. M., & Patel, C. 2016, ApJ, 827, 59
Terashima, Y., & Wilson, A. S. 2003, ApJ, 583, 145
Thornton, D., Stappers, B., Bailes, M., et al. 2013, Sci, 341, 53
Verner, D. A., Ferland, G. J., Korista, K. T., & Yakovlev, D. G. 1996, ApJ, 465, 487
Wilms, J., Allen, A., & McCray, R. 2000, ApJ, 542, 914
Yao, J. M., Manchester, R. N., & Wang, N. 2017, ApJ, 835, 29